















105 efficiency around 18-24% can be reach, depending on the initial investment. Lambert et al. [16]  
106 analyse the energy cost of CO<sub>2</sub> capture for a natural gas combined cycle plant, and the  
107 integration with a solar tower system. Different cases are studied, including the exhaust gas  
108 recirculation and the pre-combustion case that uses the exhaust gas recirculation with the  
109 capture being realized after the compression stage of the gas turbine. It was found that addition  
110 of solar energy reduces the total energy costs.

111

112 Because of the importance ISCC plants have attained, it necessary to develop simulators that  
113 model these plants to satisfy various objectives, such as the evaluation of control strategies,  
114 optimization, or planning. Cau et al. [11] used the software GateCycle® for the evaluation of  
115 ISCC plants. GateCycle® enables the design of CC plants, fossil boiler plants, cogeneration  
116 systems, combined heat and power plants, advanced cycle gas turbines, and many other energy  
117 systems. The software can be used for evaluation, design, remodeling, re-powering, and  
118 acceptance testing. However, this software does not include models of solar collectors;  
119 therefore, the authors first developed a model for solar collector plants and then evaluated a CC  
120 plant using GateCycle®. Aftzoglou [1] performed a study of an ISCC plant from the  
121 thermodynamic perspective based on the principle of overheating. For this study, the simulator  
122 CycleTempo was used. CycleTempo is a tool for the thermodynamic analysis and optimization  
123 of systems designed for the production of electricity, heat and refrigeration. It should be noted  
124 that both the GateCycle® software and the simulator proposed by Aftzoglou [1] are steady state  
125 simulators whose purpose is the design of ISCC plants. By contrast, the simulator proposed in  
126 this paper is a dynamic simulator for the design and dimensioning of ISCC plants, the study  
127 and design of control strategies, and dynamic optimization. Thus, this paper presents a new  
128 and, to the best of our knowledge, unique contribution to ISCC plant design because no other



129 dynamic simulator of this type has yet been reported in the literature.

130

## 131 **2. Plant Description**

132 The ISCC power plant analyzed in this study corresponds to the integration of a CC plant with  
133 both a supplementary fired boiler and a distributed solar collector plant. The idea is to replace  
134 some fraction of the steam produced by the supplementary fired boiler with steam produced in  
135 a steam generator that uses oil heated in a solar collector plant. The integration of the solar  
136 plant into the CC plant was achieved following the study by Kelly et al. [15].

137

### 138 **2.1 Combined Cycle Power Plants**

139 In a CC power plant, a gas turbine and a steam turbine are used to generate electrical power. The  
140 exhaust gas from the gas turbine is used to generate steam in the boiler. The boiler extracts heat  
141 from the exhaust gas to increase the temperature and pressure of the steam. In a CC plant with a  
142 supplementary fired boiler, in addition to the heat recovered from the exhaust gas, an additional  
143 firing is provided to the boiler, thereby increasing the amount of steam produced. The electrical  
144 efficiency may be lower than that of the standard configuration (without a supplementary firing  
145 to the boiler), but there is additional flexibility in that the boiler may be supplied with a different  
146 type of fuel from that of the turbine [18].

147

### 148 **2.2 Solar Collector Plants**

149 The solar power plant considered in this paper is a solar thermal plant featuring parabolic  
150 collectors. The parameters considered in the simulator emulate the operation of the real plant

151 located in the desert of Tabernas, Southern Spain. The plant consists of a field of 480  
152 distributed solar collectors grouped into 20 rows and 10 parallel loops. Each loop has a length  
153 of 172 m, and the total open surface area is 2672 m<sup>2</sup>. The primary objective of this type of solar  
154 plant, namely, one based on a distributed collector field, is to collect solar energy by heating oil  
155 that is passing through the field. The field is also provided with a tracking system, which causes  
156 the mirrors to revolve around an axis parallel to the pipe, thereby enabling the collectors to  
157 reduce the angle between the rays of the sun and a vector normal to the aperture of the collector  
158 (angle of incidence). Cold inlet oil is extracted from the bottom of the storage tank and passed  
159 through the field by a pump located at the field inlet. This fluid is heated and then returned to  
160 the storage tank. The type of oil used in this plant is Santotherm 55. The operating temperature  
161 range is -25 °C to 290 °C. In many parts of the world, especially Europe, Solutia markets  
162 Therminol 55 HTFs under the name of either Santotherm 55 or Gilotherm 55. This fluid has a  
163 low thermal conductivity, and its density is highly dependent on temperature. One storage tank  
164 can be used to contain both hot and cold oil. The tank used in this field has a capacity of 140  
165 m<sup>3</sup>, which allows for the storage of 2.3 thermal MWh; it has an inlet temperature of  
166 approximately 210 °C and an outlet temperature of approximately 290 °C [8].

167

### 168 **3. The ISCC Dynamic Simulator**

169 A dynamic simulator for a combined cycle power plant with integrated solar collectors (i.e., an  
170 ISCC plant) was developed using MATLAB/Simulink®. The design is based on a simulator for  
171 a solar collector plant, ACUREX [8], and on the combined cycle plant simulator developed by  
172 Sáez et al. [22], which is based on the phenomenological equations presented by Ordys et al.  
173 [17]. This simulator is useful for studying the behavior of variables relevant to an ISCC plant,

174 for comparing the dynamics of an ISCC plant with those of a CC plant and for ISCC plant  
 175 design. Among the relevant variables to consider are the fuel flow from the furnace, the drum  
 176 level, the steam pressure in the superheater and the furnace gas pressure. The simulator is also  
 177 designed to assess the reduction in the fuel consumption of the furnace relative to the fuel  
 178 consumption of CC plants. The simulator was developed for a 45 MW combined cycle thermal  
 179 power plant consisting of a boiler, a  $P_s=11$  MW steam turbine and a  $P_g=34$  MW gas turbine.  
 180 The available simulator for the ACUREX solar plant is able to deliver a peak thermal power of  
 181 1.2 MW. Various representative examples of ISCC plants can generate higher power. In this  
 182 paper, the primary objective of the scale test simulator is to reproduce the most relevant  
 183 phenomenological processes of ISCC plants. For the integration of a solar plant and a solar  
 184 steam generator (SSG) into a combined cycle plant, it is necessary to add certain equipment,  
 185 such as pumps and valves, in addition to adapting the equations that describe the dynamics of  
 186 the CC plant superheater. The equations that describe the dynamics of the drum do not change.  
 187 According to Ordys et al. [18], the equations for the drum are as follows:

$$188 \quad w_e + (1-x)w_r - w_d - w_{ec} = \frac{d}{dt}(m_{d1}) \quad (1)$$

$$189 \quad \frac{m_{d1}}{\rho_w} = f(L) \quad L = f^{-1}\left(\frac{m_{d1}}{\rho_w}\right)$$

$$190 \quad V_L = f(L) = \pi r^2 L \quad (2)$$

$$191 \quad w_d = v_{dow} \rho_w \quad (3)$$

$$192 \quad w_e h_e + (1-x)w_r h_{rv} = w_d h_w + w_{ec} h_v + \frac{d}{dt}(m_{d1} h_w) \quad (4)$$

193 
$$w_{ec} + xw_r - w_v = \frac{d}{dt}(V_v \rho_v) \quad (5)$$

194 
$$w_{ec} = K_{ec}(T_w - T_v) \quad (6)$$

195 
$$V_v = V - V_l \quad (7)$$

196 where equation (1) represents the liquid mass balance, (2) the drum liquid level, (3) the  
197 downcomer mass flow, (4) the liquid heat balance, (5) the steam mass balance, (6) the  
198 evaporation dynamics and (7) the vapor volume.

199

200 In designing the dynamic simulator for an ISCC plant, the following assumptions were  
201 adopted:

- 202 - The solar plant has its own field controller that keeps the outlet oil set point temperature  
203 for changing weather conditions. This controller adjusts the oil flow in the solar field in  
204 order to reject the disturbances caused by the variation of solar radiation along the day and  
205 changes in the return inlet oil temperature. The solar plant has a storage tank which  
206 provides energy from which the oil that passes to the solar steam generator is extracted and  
207 decouples both parts of the plant. So, although the oil flow is not fixed (since it is  
208 continually manipulated by the solar field controller), the solar support can be considered  
209 constant. Therefore, when the solar field is in operation, the thermal energy supplied by the  
210 storage tank is kept at its nominal value.
- 211 - From the previous assumption, it follows that the temperature of the oil inlet to the solar  
212 steam generator can be held constant during day-to-day planning operations.
- 213 - The water mass flow from the feed water to the drum in the CC plant is the same as the  
214 water mass flow from the feed water to the drum in the ISCC plant.

- 215 - The gas turbine and the steam turbine are similar in both the CC and ISCC simulators. The  
216 only difference is the source of energy used to heat the steam.
- 217 - Basic PI controllers are considered because they are typically implemented efficiently in  
218 real plants for the control of steam pressure, drum level, furnace gas pressure, superheated  
219 steam temperature, exhaust gas temperature,  $\text{NO}_x$  concentration in exhaust gas and turbine  
220 mechanical power. Thus, the PI control loops of the ISCC plant simulator are similar to  
221 those of the CC plant simulator. A feedforward controller is incorporated for the feed water  
222 supplied to the SSG.

223

### 224 **3.1 Design of the Solar Steam Generator Simulator**

225 An SSG uses oil that was previously heated in a solar collector plant and then stored in an  
226 energy storage tank. The heat of the oil is transferred to liquid water, producing steam that then  
227 passes into the combined cycle plant. The oil from the solar plant has a certain temperature  $T_a$   
228 and a given mass flow  $m_a$ . The inlet liquid water in the SSG has an enthalpy  $h_w$  and a  
229 temperature  $T_w$ , but as it flows through the heat exchanger and the water is heated to the  
230 saturated steam temperature corresponding to the inlet flow pressure  $p_{eg}$ , saturated steam with a  
231 steam enthalpy of  $h_{gm}$  is produced. Subsequently, the output emits a steam flow that  
232 corresponds to  $w_{gm}$  and a heat flow of  $Q_{gm}$ . Fig. 2 shows a schematic diagram of the heat  
233 interchange process between the oil from the storage tank of the solar plant and the water from  
234 the heat recovery steam generator (HRSG) of the CC plant.

235

236 As described by Dersch et al. [12], Price et al. [19] and Kelly et al. [15], the SSG was designed  
237 by considering an inlet water flow of 10% of the water flow injected into the drum of the CC  
238 plant.

239

240 The characteristics of the oil from the ACUREX solar collectors were also considered, i.e., the  
241 specific heat, temperature and mass flow of the oil. Fig. 3 presents a diagram that depicts the  
242 inputs and outputs of the SSG simulator. The inlet water mass flow pressure  $p_{eg}$  is derived from  
243 the pump used to increase the water flow pressure from the feed water (Fig. 1), and saturated  
244 steam is obtained in the SSG. The equations that describe the SSG are as follows:

$$245 \quad C_{pa} = 1820 + 3.478T_a \quad (8)$$

$$246 \quad T_0 = \frac{3816.4}{18.304 - \ln(p_{vgm})} + 46.13 \quad (9)$$

$$247 \quad h_{gm} = -1.8934 \cdot 10^6 + 4.1404 \cdot 10^4 T_0 - 148.7585 \cdot T_0^2 + 0.2471 \cdot T_0^3 - 1.5519 \cdot 10^{-4} \cdot T_0^4 \quad (10)$$

$$248 \quad Q_a = m_a C_{pa} (T_a - T_0) \quad (11)$$

$$249 \quad Q_{gm} = -Q_a \quad (12)$$

$$250 \quad \frac{d}{dt} w_{gm} = (w_{eg} - w_{gm}) / \tau_g \quad (13)$$

251 where (8) to (12) are algebraic equations and (13) a differential equation. Equation (8)  
252 describes the specific heat of the oil Therminol 55 as a function of its temperature. Other  
253 properties of the oil, such as its thermal conductivity, dynamic viscosity and Prandlt number,  
254 also depend on the temperature [9], [10]. Equation (9) is the steam saturation temperature as  
255 described by Reid et al. [20]. Saturated steam is produced at a high temperature and then enters  
256 the superheater. Equation (10) represents the enthalpy of saturated steam as a function of the

257 steam temperature, as suggested in a study conducted by Reynolds [21]. In Equation (11), the  
258 heat transferred to the oil from solar radiation is a function of the oil temperature and the steam  
259 saturation temperature. Equation (12) is a heat balance, heat received by the steam in the heat  
260 exchanger is equal to the heat provided by the oil; thus, heat losses are negligible. The steam  
261 flow at the outlet of the steam generator ( $w_{gm}$ ) can be obtained using equation (13), where the  
262 speed of the steam flow equals the difference between the inflow to and outflow from the  
263 exchanger divided by a time constant ( $\tau_g$ ).

264

265 In the SSG simulation process, the values of  $T_a$  and  $m_a$  from the solar plant are read.  $w_{eg}$  and  $p_{eg}$   
266 are also read, where the first variable is derived from the feed water and the second is obtained  
267 from the pump installed at the outlet of the feed water. The initial SSG conditions and  
268 parameters are defined. Algebraic equations (8) to (12) are solved. Then,  $w_{gm}$  is obtained via  
269 equation (13) using  $w_{eg}$  and  $\tau_g$ . The values obtained for  $h_{gm}$ ,  $Q_{gm}$ ,  $T_o$  and  $w_{gm}$  are applied to the  
270 superheater. This loop is repeated at each sampling time step. The attemperator is part of the  
271 superheater. The inflow to the superheater is  $w_T$ , whereas  $w_s$  corresponds to the outflow of the  
272 superheater, which is the steam at the input to the turbine. Both are shown in Fig. 3.

273

274 In Fig. 3 the control loop in the drum regulates its level by opening or closing the valve when  
275 the level is lower or higher than the reference. The control loop in the steam turbine keeps the  
276 turbine power near the power reference demand by changing the flow of steam coming from  
277 the superheater. If power demand increases, the valve is opened to increase the mass flow of  
278 superheated steam. If the power demand decreases, the valve is closed to reduce the steam  
279 flow. The water supply of the steam generator also has a control loop and it works similarly to

280 the control level of the drum. The reference value in this case corresponds to the amount of  
281 liquid water that could be converted into steam in the SSV.

282

### 283 3.2 Design of the ISCC Simulator

284 As previously stated, the design of the ISCC simulator considered in this study is based on the  
285 CC simulator developed by Sáez et al. [22] with the integration of a solar plant [8]. The same  
286 equipment is considered in the design of both the CC and solar plants, with the only difference  
287 being the energy source that heats a fraction of the steam going to the superheater. In general,  
288 the models were developed using the basic principles of conservation of energy, mass and  
289 momentum. The SSG output steam,  $w_{gm}$ , is injected into the boiler of the combined cycle plant  
290 in the superheater stage. The injected steam is added to the steam from the drum  $w_v$ . All steam  
291 present in the superheater,  $w_T$ , is heated to a superheated state. Finally, the superheated steam,  
292  $w_s$ , is injected into the steam turbine in the high-pressure section (HP). The equations that  
293 describe the dynamics of the superheater are as follows:

294

$$295 \quad p_v - p_s = \frac{w_T^2}{\rho_T} f_s \quad (14)$$

$$296 \quad Q_s = k_s w_T^{0.8} (T_{st} - T_s) \quad (15)$$

$$297 \quad \begin{aligned} \Delta h &= C_{ps} (T_s - T_{ref}) \\ T_s &= (h_s - h_{ref}) / C_{ps} + T_{ref} \end{aligned} \quad (16)$$

$$298 \quad p_s = R_s \rho_s T_s \quad (17)$$

$$299 \quad w_v C_v (T_t - T_v) = w_{gm} C_{gm} (T_{gm} - T_t) \quad (18)$$



$$300 \quad T_t = \frac{w_v T_v + w_{gm} T_{gm}}{w_v + w_{gm}} \quad (19)$$

$$301 \quad w_v - w_s + w_{gm} + w_{at} = V_s \frac{d}{dt}(\rho_s) \quad (20)$$

$$302 \quad Q_{gs} + Q_{gm} = Q_s + M_s C_{st} \frac{d}{dt}(T_{st}) \quad (21)$$

$$303 \quad Q_s + w_v h_v + w_{gm} h_{gm} = w_s h_s - (h_a - h_f) \cdot w_{at} + V_s \frac{d}{dt}(\rho_s h_s) \quad (22)$$

304 where (14) to (19) are algebraic equations, and (20) to (22) are differential equations. The  
 305 losses due to friction that are generated in the pipelines where the total steam ( $w_T$ ) passes to the  
 306 steam turbine are estimated based on momentum balance in equation (14). Equation (15) was  
 307 empirically deduced and describes the heat transfer between the metal (pipelines) and the  
 308 steam, considering turbulent flow. As in equation (14), the total steam is considered in the  
 309 relation. The superheated steam temperature is obtained using equation (16), where the  
 310 variation in the enthalpy between a temperature  $T_s$  and the reference temperature  $T_{ref}$  is  
 311 calculated under the assumption of ideal conditions. Assuming an ideal gas model, where  $R_s$  is  
 312 the universal gas constant, the superheated steam pressure is obtained in equation (17). The  
 313 total steam generated in the superheater originates from two sources, the SSG and the exhaust  
 314 gas turbine. The temperatures of these two sources are different. A mixture of both flows must  
 315 be considered in the energy balance, as in equation (18). Under the assumption of a constant  
 316 heat capacity  $C_v \approx C_{gm}$ , the temperature of the inlet steam that arrives at the superheater is  
 317 obtain using equation (19). Through mass balance, the total steam in the superheater is  
 318 obtained in equation (20). The inflow is equal to the outflow of the superheater; thus, losses are  
 319 negligible. Note that in (20), an average behavior of density along the pipe is considered. This

320 assumption could be relaxed and in a future work the steam density changes along the pipe  
321 could be modelled. In equation (21) is the superheater heat balance. The heat that is transferred  
322 to the steam, according to the furnace model, incurs losses in the pipelines through which the  
323 steam flows (final term of the equation). The heat balance equation (22) for steam includes the  
324 energy provided by the steam from the SSG; therefore, this balance equation is different from  
325 that presented by Sáez et al. [22].

326

327 In the first step of the superheater simulation process,  $w_a$ ,  $w_s$ ,  $p_v$ ,  $Q_{gs}$ ,  $h_v$ ,  $h_o$ ,  $w_{gm}$ ,  $h_{gm}$ ,  $Q_{gm}$ ,  $T_{gm}$ ,  
328 and  $T_o$  are measured. The superheater parameters are defined, and the initial conditions for  $xsI$ ,  
329  $h_s$  and  $p_s$  are provided. Then,  $xsI$  is calculated. Algebraic equations (14) to (19) are solved.  
330 Then, differential equations (20) to (22) are solved.  $P_s$ ,  $T_s$ ,  $h_s$ , and  $\rho_s$  are sent to the steam  
331 turbine. The loop is repeated at each sampling time. Other routines used in the simulator have  
332 already been implemented and reported by Ordys et al. [18] and Sáez et al. [22]. At the  
333 beginning of the paper, the nomenclature and the variable ranges used in the simulators are  
334 specified.

335

#### 336 **4. Model Predictive Control at the Supervisory Level for an ISCC Plant**

337 A Model Predictive Control (MPC) strategy at the supervisory level for ISCC plants was  
338 designed. The output of the supervisory level scheme is used as a set point for the steam  
339 pressure in the boiler at the regulatory level. Fig. 4 illustrates a scheme for such a control  
340 strategy. The external set point  $p_s^*$  is constant and corresponds to the steady-state superheater  
341 steam pressure.

342

343 The output variables of the boiler are the furnace pressure of the gases ( $p_G$ ), the temperature of  
 344 the steam at the outlet of the boiler ( $T_S$ ) and the level of the drum of the CC plant ( $L$ ). These  
 345 variables are controlled using PI controllers at the regulatory level. For the supervisory control  
 346 strategy, the input is  $p_s$  and the output is  $p_s^r$ .

347

#### 348 **4.1 System Identification**

349 For the supervisory-level model, an ARIX (Auto-Regressive Integrated with Exogenous input)  
 350 model was established for the outlet pressure of the steam flow of the superheater,  $p_s$ , as a  
 351 function of the fuel flow of the afterburner,  $w_F$ . For the design of the supervisory-level control  
 352 scheme, a data set was obtained from the simulator by varying the reference pressure ( $p_s^r$ ) and  
 353 adding pseudorandom binary noise. The reference values were varied between  $3.5 \times 10^6$  and  
 354  $5.4 \times 10^6$  Pa. Furthermore, a model for the regulatory-level PI controllers was obtained for the  
 355 fuel flow  $w_F$  as a function of  $p_s^r$ . The sampling time of this model is  $t_m = 10$  s, and its structure  
 356 is as follows:

$$357 \quad A(z^{-1})p_s(t) = B(z^{-1})w_F(t) + \frac{e(t)}{\Delta} \quad (23)$$

358 where  $e(t)$  is white noise;  $z^{-1}$  is the delay operator,  $z^{-1}y(t) = y(t-1)$ ;  $\Delta = 1 - z^{-1}$ ; and the  
 359 polynomials  $A(z^{-1})$  and  $B(z^{-1})$  are of 13<sup>th</sup> order:

$$360 \quad A(z^{-1}) = 1 + a_1z^{-1} + a_2z^{-2} + a_3z^{-3} + a_4z^{-4} + a_5z^{-5} + a_6z^{-6} + a_7z^{-7} + a_8z^{-8} +$$

$$a_9z^{-9} + a_{10}z^{-10} + a_{11}z^{-11} + a_{12}z^{-12} + a_{13}z^{-13}$$

$$361 \quad B(z^{-1}) = b_1z^{-1} + b_2z^{-2} + b_3z^{-3} + b_4z^{-4} + b_5z^{-5} + b_6z^{-6} + b_7z^{-7} +$$

$$b_8z^{-8} + b_9z^{-9} + b_{10}z^{-10} + b_{11}z^{-11} + b_{12}z^{-12} + b_{13}z^{-13}$$

362 This model was obtained by evaluating the RMS errors between the actual values and the  
 363 values obtained using ARIX models of different orders (structure optimization). The model  
 364 with the lowest RMS error was thus selected. To calculate the control variable  $w_F$ , a PI  
 365 controller is considered as follows:

$$366 \quad w_F(s) = \left( K_p + \frac{K_i}{s} \right) (p_s^r(s) - p_s(s)) \quad (24)$$

367 where  $K_p = 3 \times 10^{-6}$ ,  $K_i = 2 \times 10^{-8}$ ,  $p_s^r(s)$  is the reference pressure for the superheated steam, and  
 368  $p_s(s)$  is the real pressure of the superheated steam.

369

## 370 4.2 Objective Function

371 The objective function used for the supervisory MPC strategy is given by

$$372 \quad J = J_{cr} + \lambda J_{cf} \quad (25)$$

$$373 \quad J_{cr} = \alpha \sum_{k=1}^N (\hat{p}_s(t+k) - p_s^*)^2 + \beta \sum_{k=1}^N \Delta w_F^2(t+k-1) \quad (26)$$

$$374 \quad J_{cf} = \sum_{k=1}^N C_f w_F(t+k-1) \quad (27)$$

375 and the following operational constraints over the fuel flow are included:

$$376 \quad 10 \leq w_F(t+k-1) \leq 14.5, \quad k = 1, \dots, N \quad (28)$$

377 where  $\hat{p}_s(t+k)$  is the k-step-ahead prediction for the reference pressure,  $w_F(t+k-1)$  is the fuel  
 378 flow and  $\Delta w_F(t+k-1)$  is the control effort at instant  $t+k-1$ . The first term in equation (25) is a

379 regulatory term, whereas the second term optimizes the fuel costs. In equation (26), the second  
380 term accounts for the optimization of the control effort together with the tracking error. In  
381 equation (27),  $C_f$  is the fuel cost per flow unit in US\$/(kg/s). The minimum and maximum  
382 values defined in constraint equation (28) are chosen from [18] and they correspond to the  
383 constraints over the start-up and the maximum admissible fuel flow of the CC plant. Finally,  
384 the decision variable  $p_s^r$  is obtained by minimizing the objective function of equation (25),  
385 considering the corresponding constraints and using the PI controller model given by equation  
386 (28).

387

### 388 4.3 Parameter Tuning of the Supervisory MPC Strategy

389 In equations (25) and (26), the weights ( $\lambda$ ,  $\alpha$ ,  $\beta$ ) are obtained from the design of the objective  
390 function. Each of these weights represents the relative importance of the function by which it is  
391 multiplied. To optimize these variables, we adopted a simulation-based approach in which, for  
392 a fixed value of  $\beta=1$ , different values of  $\alpha$  and  $\lambda$  were tested over the entire simulation period.  
393 A broad range of values were evaluated. Based on global performance statistics, the optimal  
394 tuning parameters were obtained; in this case, these parameters were found to be  $\alpha=10^8$  and  
395  $\lambda=10^2$ . To consider the performance of the system over the entire simulation period  $t_{sim}$ , each  
396 pair of parameters was assessed based on global statistics:

$$397 \quad \overline{J} = \frac{1}{t_{sim}} \sum_{k=1}^{t_{sim}} J(k) = \frac{1}{t_{sim}} \sum_{k=1}^{t_{sim}} (J_{Cr}(k) + \lambda J_{Cf}(k)) \quad (29)$$

$$398 \quad \overline{J}_{Cr} = \frac{1}{t_{sim}} \sum_{k=1}^{t_{sim}} J_{Cr}(k) \quad (30)$$

399 
$$\overline{J}_{cf} = \frac{1}{t_{sim}} \sum_{k=1}^{t_{sim}} J_{cf}(k) \quad (31)$$

400 where equation (29) is the global performance index for the total objective function, equation  
401 (30) is the global performance index for the regulatory term, and equation (31) is the global  
402 index for the fuel cost. Using these parameters, good overall controller performance was  
403 achieved, with a reasonable trade-off between the tracking error on the pressure of the steam in  
404 the boiler and the reference value given by the supervisory MPC scheme, while maintaining  
405 minimal burning of the fuel at the auxiliary burner.

406

#### 407 **4.4 Performance Index**

408 To compare the fuel consumption between a CC plant and an ISCC plant, the amount of fuel  
409 saved is defined as the amount of fuel consumed by the CC plant minus the amount of fuel  
410 consumed by the ISCC plant; under the assumption that the amount of fuel used by the CC  
411 plant corresponds to 100%, the percent reduction in the amount of fuel supplied to the furnace  
412 is calculated as the amount of fuel consumed by the CC plant minus the amount of fuel  
413 consumed by the ISCC plant, divided the amount of fuel consumed by the CC and multiplied  
414 by 100. To compare the performance of the ISCC plant with and without the implementation of  
415 the supervisory MPC strategy, the following global indicator of the fuel used at the auxiliary  
416 burner was defined:

417 
$$I_{wF} = \frac{1}{t_{sim}} \sum_{k=1}^{t_{sim}} w_F(k) \quad (32)$$

418

419

## 420 **5. Simulation Results**

### 421 **5.1 Comparison of the ISCC Plant with the CC Plant**

422 To validate the behavior of the ISCC plant simulator, several simulations were performed, as  
423 many with the ISCC simulator as with the CC simulator. The results obtained for different  
424 cases and using different variables were compared. The behaviors of both the controlled and  
425 manipulated variables of the boiler were studied. The controlled variables that were studied  
426 included the steam pressure in the superheater,  $p_s$ ; the drum level,  $L$ ; the pressure of the gases in  
427 the furnace,  $p_G$ ; and the temperature of the superheated steam in the superheater,  $T_s$ . The  
428 manipulated variables that were studied included the flow of fuel from the auxiliary burner of  
429 the furnace,  $w_F$ ; the water flow from the economizer,  $w_e$ ; the air flow from the auxiliary burner  
430 of the furnace,  $w_A$ ; and the mass flow of water from the attemperator,  $w_{at}$ . Manipulated  
431 variables are also known as decision variables. The purpose was to optimize those variables  
432 such that the ISCC plant exhibited both good tracking performance and reduced fuel costs. Two  
433 cases are presented: one in which a supervisory controller was used, and one in which a PI  
434 controller was used. To illustrate the behavior of the controllers, a step-function change in the  
435 reference value of the steam pressure was applied, and the dynamic response is presented in  
436 Fig. 5. After 40 s approx., the transient responses are observed for both controllers achieving  
437 the new set-point. The overshoot is lower with the supervisory controller compared with the PI  
438 control strategy.

439

440 A downward step of 10% was applied to the set point of the gas turbine power ( $P_G^*$ ) and to the  
441 set point of the steam turbine power ( $P_s^*$ ). This downward step was applied in three different  
442 cases: first for the CC plant simulator, then for the ISCC plant simulator with 10% steam

443 support from the SSG and, finally, for the ISCC plant simulator with 20% solar support. The  
444 objective of these simulations was to vary the behavior of the controlled and manipulated  
445 variables pertaining to the furnace before the addition of steam support from the SSG and, in  
446 particular, to verify that the flow of fuel,  $w_F$ , diminishes when solar plant support is added. Fig.  
447 6 shows the results obtained for the controlled variables of the boiler when  $P_s^*$  (the steam  
448 turbine power set point) was varied in both simulations. Fig. 7 shows the results obtained for  
449 the manipulated variables when  $P_s^*$  was varied. As we expected, the variables return to the set-  
450 points for all cases. A slight increase is observed for steam pressure of the superheater when the  
451 20% steam support is considered. The fuel flow as well as air flow decrease when the steam  
452 support increase, because less steam from the HRSG is required. On the contrary, water flow  
453 from the economizer increases. Fig. 8 shows the results obtained for the controlled variables  
454 when  $P_G^*$  (the gas turbine power set point) was varied in both simulations. When a step change  
455 is applied to the gas turbine power, the variable will return to its set-point because the same  
456 local control strategy is considered for both CC and ISCC cases. Fig. 9 shows the results  
457 obtained for the manipulated variables in this latter case. The controlled variables return to the  
458 set-points for all cases. The fuel flow is reduced when the steam support increased, because less  
459 steam produced by HRSG is required.

460

461 Figs. 7 and 9 show that the ISCC plant demonstrates lower fuel consumption,  $w_F$ . This result  
462 holds whether the variation in power demand occurs in the gas turbine or in the steam turbine.  
463 The fuel consumption decreases as the steam contribution from the solar plant increases. Figs. 6  
464 and 8 also illustrate that the water level of the drum,  $L$ , in the ISCC plant remains constant as  
465 the steam supply from SSG varies (for variations of 10% or 20%). The pressure of the steam in



466 the superheater does not change as the extent of solar support increases from 10% to 20%. The  
467 gas pressure of the furnace,  $p_G$ , and the temperature of the superheated steam,  $T_s$ , remain  
468 constant as the support from the solar plant increases. The reason why these variables remain  
469 nearly constant is the different control loops that operate for each of the variables.

470 Table 1 shows the percentage fuel savings achieved when using an ISCC plant compared with a  
471 CC plant, i.e., the fuel savings realized by introducing the steam from a solar plant. This  
472 calculation was performed for solar contributions of 10%, 15% and 20%, which corresponds to  
473 possible changes of available solar contribution along the year. It is evident that the amount of  
474 fuel saved increases with increasing solar support, as expected. The fact that the simulator can  
475 compute these quantities may be very useful for the design and optimal operation of ISCC  
476 plants.

477 Fig. 10 shows the behavior of the heat flow being transferred from the furnace to the  
478 superheater ( $Q_{gs}$ ) when the ISCC plant remains constant as the steam supply from SSG varies  
479 (for variations of 10% or 20%) as well as the steam power set-point diminishes at  $t = 50$  s. It  
480 appears that the heat support provided by the furnace to the superheater that is required to  
481 produce the same power diminishes upon the addition of support provided by the solar plant.  
482 When the heat support from the solar plant is bigger, less heat support provided by the furnace  
483 to the superheater is required. Therefore, in this case, the furnace uses less fuel to produce the  
484 same amount of power. It appears that the heat support provided by the furnace to the  
485 superheater that is required to produce the same power diminishes upon the addition of support  
486 provided by the solar plant. When the heat support from the solar plant is bigger, less heat  
487 support provided by the furnace to the superheater is required. Therefore, in this case, the  
488 furnace uses less fuel to produce the same amount of power.

## 489 **5.2 Comparison of ISCC Plant Performance with Supervisory MPC and** 490 **PI Control Strategies**

491 The fuel consumption savings achieved using supervisory MPC and PI control strategies were  
492 calculated. Table 2 compares the simulation-based results obtained using the index given by  
493 equation (32), corresponding to the amount of fuel consumed over a simulation period of 500 s.  
494 Considering that an ISCC plant operates over 12 consecutive hours, because the simulator  
495 design assumes that the oil is extracted from the storage tank, the savings in fuel consumption  
496 amounts to  $\Delta w_F = 1754$  kg. Over one year of operation, this savings would be approximately  
497  $\Delta w_F = 1,280,361.6$  kg. In February 2014, the price of natural gas in Chile was 1.44 US\$/kg;  
498 thus, such a savings would amount to approximately 1,843,721 US\$/year. These results  
499 demonstrate the relevance of implementing a proper supervisory strategy, particularly when  
500 comparing a supervisory MPC strategy with the conventional PI strategy at the regulatory level.  
501 For the same power demand, fuel consumption can be better optimized using the MPC-based  
502 strategy than with a PI controller alone. It is considered that the plant operates for 24 hours  
503 because the simulator assumes that the oil is extracted from the storage tank, which allows the  
504 oil temperature to remain constant. We assumed that the SSG has a well-sized storage that is  
505 used for ensuring the supply of 24-hours.

506 The following is an analysis of the effects of changes in the reference powers for the gas  
507 turbine and the steam turbine that allows for a better understanding of how fuel consumption  
508 varies in each of these cases. Two types of variations in the reference powers of the steam  
509 turbine and the gas turbine were considered. First, the reference power was decreased by 10%  
510 and then increased by 10%. This test was performed for both the supervisory MPC strategy and  
511 the regulatory-level PI controller. Fig. 11 shows the evolutions of the steam pressure with the

512 supervisory MPC strategy ( $p_s$  supervisory), with the PI controller ( $p_s$  PI) and with the reference  
513 pressure ( $p_s^r$ ) for a decrease of 10% in the reference power of the steam turbine and in that of  
514 the gas turbine. The figure shows that the steam pressure response  $p_s$  exhibits a lower overshoot  
515 in the case of the supervisory MPC strategy for a decrease in the reference power of the steam  
516 turbine. With respect to a change in the reference power of the gas turbine, the difference  
517 between the responses of the two controllers is minimal, indicating that both strategies can  
518 successfully push the pressure of the steam flow toward its reference value. Fig. 12 shows the  
519 evolution of the manipulated variable  $w_F$  (fuel flow). It can be observed that when the power  
520 demand of the steam turbine ( $P_s^*$ ) decreases, fuel consumption also decreases. This occurs for  
521 both control strategies, but the decrease is greater in the case of a supervisory MPC strategy.  
522 That is, under the same operating conditions, less fuel is used when the plant employs a  
523 predictive control strategy. When the reference power decreases in the gas turbine, an increase  
524 in fuel flow occurs for both strategies, but in the case of the supervisory MPC strategy, the  
525 increase in fuel flow is lower.

526 Fig. 13 shows the evolution of the steam pressure in the superheater when an increase in the  
527 reference power of the steam turbine or the gas turbine occurs for both control strategies. As in  
528 the previous cases, the results demonstrate that both controllers are able to maintain the steam  
529 pressure responses within similar ranges. When the power of the gas turbine increases, less  
530 overshoot is observed for the supervisory control strategy. When the power of the steam turbine  
531 increases, the steam pressure response is similar for both controllers, but the response with the  
532 supervisory MPC strategy is faster. Fig. 14 shows the fuel consumption incurred with the  
533 supervisory MPC strategy and the regulatory-level PI controller strategy when the reference  
534 powers of the steam turbine and gas turbine are increased. When the power of the steam turbine

535 is increased, an increase in fuel consumption is observed in the auxiliary burner; however, in  
536 the case of the system controlled with a supervisory MPC scheme, this increase is much lower.  
537 Moreover, when the reference power of the gas turbine increases, the fuel consumption of the  
538 afterburner decreases, exhibiting a greater reduction in the case of the supervisory-MPC-  
539 controlled system. Thus, the fuel consumption is greater when PI control at the regulatory level  
540 is applied.

541 Table 3 summarizes the savings in fuel consumption achieved by changing the reference values  
542 of the steam and gas turbines. The index  $I_{WF}$  was calculated using equation (32). Additionally,  
543 the differences in fuel consumption between the two control strategies are presented in terms of  
544 net values and percentages. In Table 3, a negative sign (-) represents a decrease in the set point  
545 and a positive sign (+) represents an increase in the set point.

546

## 547 **6. Conclusions**

548 A dynamic simulator for a combined cycle plant with integrated solar collectors (ISCC plant)  
549 was developed. The results obtained from the simulations were compared with the results  
550 obtained from simulations of the combined cycle plant alone. Simulations for both cases were  
551 performed first with 10% support from a steam flow from the solar plant and then with 20%  
552 solar support. In both cases, the results were compared with the values obtained for the  
553 combined cycle plant. Among the main results obtained, it was observed that an increase in the  
554 steam support from the solar plant diminishes the flow of fuel from the furnace. The flow of  
555 heat delivered by the furnace to the superheater diminishes with an increase in the mass flow of  
556 steam provided by the solar plant. The supervisory MPC strategy developed for the steam  
557 pressure in the superheater allows for the optimization of the fuel flow in the auxiliary burner,

558 thereby allowing the same steam pressure obtained using a PI control strategy to be produced  
559 with less fuel consumption for the same power demand. The results demonstrate that in general,  
560 fuel consumption is lower under the supervisory MPC strategy. The greatest differences are  
561 observed when there is a decrease in the power of the steam turbine and when there is an  
562 increase in the power of the gas turbine. The developed simulator is suitable for the study and  
563 design of control strategies, for determining the sizing of equipment and for the dynamic  
564 optimization of ISCC plants. Further research will focus on multivariable MPC control  
565 strategies for ISCC plants and an analysis of the robustness of the MPC controller.

566

## 567 **Acknowledgments**

568 This work was partially supported by the Solar Energy Research Center (SERC) through  
569 CONICYT: FBO16 and CONICYT/FONDAP/15110019. CVP is grateful for the support  
570 provided by CONICYT-Chile through a doctorate scholarship and to the University of La  
571 Serena for study leave.

572

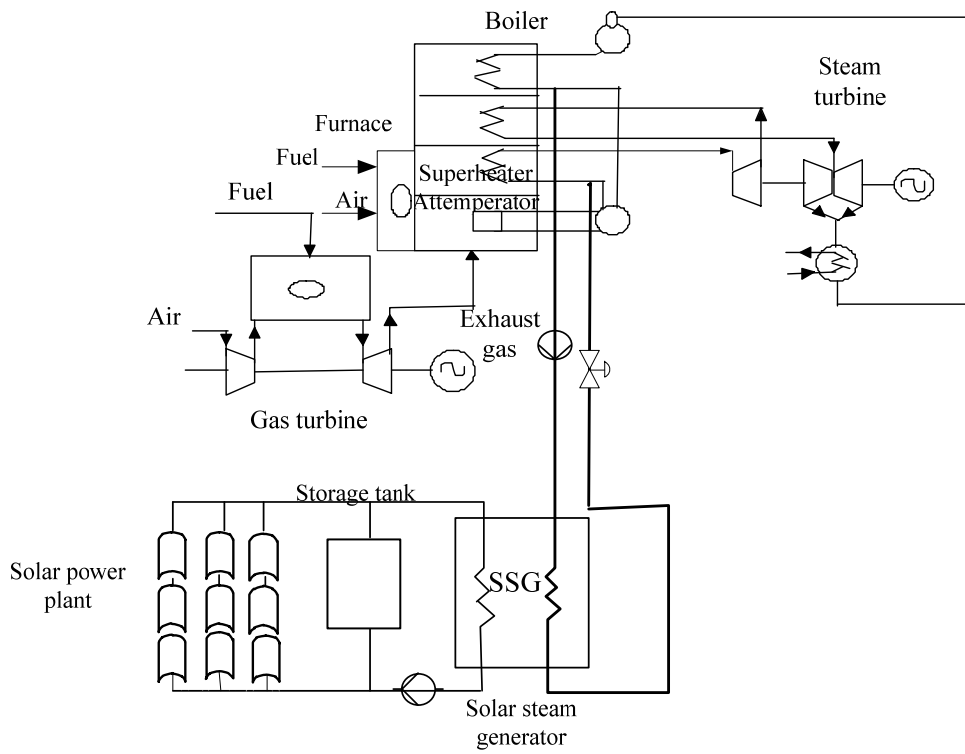
## 573 **References**

- 574 [1] Aftzoglou, Z., 2011. Exploring Integration Options in the Energy Sector, Including a Case Study of the  
575 Integration of Solar Thermal Energy into a Combined Cycle Power Plant, MSc Thesis, Delft University of  
576 Technology, Delft, The Netherlands.
- 577 [2] Amelio, M., Ferraro, V., Marinelli, V. and Summaria, A., 2014. An evaluation of the performance of an  
578 integrated solar combined cycle plant provided with air-linear parabolic collectors. *Energy*, 69:742-748. DOI:  
579 10.1016/j.energy.2014.03.068
- 580 [3] Al-Sulaiman, F. 2014. Exergy Analysis of Parabolic Trough Solar Collectors Integrated with Combined  
581 Steam and Organic Rankine Cycle. *Energy Conversion and Management*, 77:441-449.  
582 DOI:10.1016/j.enconman.2013.10.013
- 583 [4] Baghernejad, A. and Yaghoubi, M., 2010. Exergy Analysis of Integrated Solar Combined Cycle System.  
584 *Renewable Energy*, 35(10): 2157-2164. DOI:10.1016/j.renene.2010.02.021
- 585 [5] Baghernejad, A. and Yaghoubi, M., 2011. Exergo-economic Analysis and Optimization of Integrated Solar  
586 Combined Cycle System (ISCCS) Using Genetic Algorithm. *Energy Conversion and Management*, 52(5):  
587 2193-2203. DOI: 10.1016/j.enconman.2010.12.019

- 588 [6] Behar, O., Kellaf, A., Mohamedi, K. and Belhamel, M., 2011. Instantaneous Performance of the First  
589 Integrated Solar Combined Cycle System in Algeria. *Energy Procedia*, 6: 185-193. DOI:  
590 10.1016/j.egypro.2011.05.022
- 591 [7] Behar, O., Kellaf, A., Mohammedi, K. and Ait-Kaci, S., 2014. A Review of Integrated Solar Combined  
592 Cycle Systems (ISCCS) with a Parabolic Through Technology. *Renewable and Sustainable Energy Reviews*,  
593 39: 223-250. DOI: 10.1016/j.rser.2014.07.066
- 594 [8] Camacho, E.F, Berenguel, M., and Rubio, F.R., 1993. Simulation Software Package of the Acurex Field,  
595 E.S.I. of Sevilla, Internal Report, Sevilla.
- 596 [9] Camacho, E., Berenguel, M. and Rubio, M., 1997. *Advanced Control of Solar Plants*. Springer-Verlag,  
597 London.
- 598 [10] Camacho, E.F., Berenguel Soria, M., Rubio, F.R., Martínez, D., 2012. *Control of Solar Energy Systems*.  
599 Springer.
- 600 [11] Cau, G., Cocco, D. and Tola, V., 2012. Performance and Cost Assessment of Integrated Solar Combined  
601 Cycle Systems (ISCCSs) Using CO<sub>2</sub> as Heat Transfer Fluid. *Solar Energy*, 86(10): 2975-2985. DOI:  
602 10.1016/j.solener.2012.07.004
- 603 [12] Dersch, J., Geyer, M., Herrmann, U., Jones, S., Kelly, B., Kistner, R., Ortmanns, W., Pitz-Paal, R., and Price,  
604 H., 2004. Trough Integration into Power Plants - a Study- on the Performance and Economy of Integrated  
605 Solar Combined Cycle Systems. *Energy*, 29(5-6): 947-959. DOI: 10.1016/S0360-5442(03)00199-3
- 606 [13] Horn, M., Furing, H. and Rheinländer, J., 2004. Economic Analysis of Integrated Solar Combined Cycle  
607 Power Plants: A Sample Case: The Economic Feasibility of an ISCCS Power Plant in Egypt. *Energy*, 29(5-  
608 6): 935-945. DOI: 10.1016/S0360-5442(03)00198-1
- 609 [14] Hosseini, R., Soltani, M. and Valizadeh, G., 2005. Technical and Economic Assessment of the Integrated  
610 Solar Combined Cycle Power Plants in Iran. *Renewable Energy*, 30(10): 1541-1555. DOI:  
611 10.1016/j.renene.2004.11.005
- 612 [15] Kelly, B., Herrmann, U. and Hale, M.J., 2001. Optimization Studies for Integrated Solar Combined Cycle  
613 Systems. *Proceeding of Solar Forum 2001*, *Solar Energy: The Power to Choose*, Washington DC, USA,  
614 April 21-25 2001.
- 615 [16] Lambert, T., Hoadley, A. and Hooper, B., 2014. Process integration of solar thermal energy with natural gas  
616 combined cycle carbon capture. *Energy*, 74:248-253. DOI: 10.1016/j.energy.2014.06.038
- 617 [17] Nezammahalleh, H., Farhadi, F. and Tanhaemami, M., 2010. Conceptual Design and Techno-economic  
618 Assessment of Integrated Solar Combined Cycle System with DSG Technology. *Solar Energy*, 84(9): 1696-  
619 1705. DOI: 10.1016/j.solener.2010.05.007
- 620 [18] Ordys, A., Pike, A., Johnson, M. and Katebi, R., 1994. *Modelling and Simulation of Power Generation*  
621 *Plants*. Springer-Verlag, London.
- 622 [19] Price, H., Lüpfert, E., Kearny, D., Zarza, E., Cohen, G., Gee, R., Mahoney, R., 2002. Advances in Parabolic  
623 Trough Solar Power Technology. *Journal of Solar Energy Engineering*, 124(2): 109-125. DOI:  
624 10.1115/1.1467922
- 625 [20] Reid, R., Prausnitz, J. & Poling, B., 1987. *Properties of Gases and Liquids*. Nueva York: McGraw-Hill Co.
- 626 [21] Reynolds, W., 1979. *Thermodynamic Properties in SI*, USA: Mechanical Eng. Dept. Stanford University.
- 627 [22] Sáez, D., Cipriano, A. and Ordys, A., 2002. *Optimization of Industrial Processes at Supervisory Level*.  
628 Application to Control of Thermal Power Plants. Springer-Verlag, London.
- 629 [23] Spelling, J., Favrat, D., Martin, A. and Augsburg, G., 2012. Thermoeconomic optimization of a combined-  
630 cycle solar tower power plant. *Energy*, 41(1): 113-120. DOI: 10.1016/j.energy.2011.03.073

631  
632  
633  
634

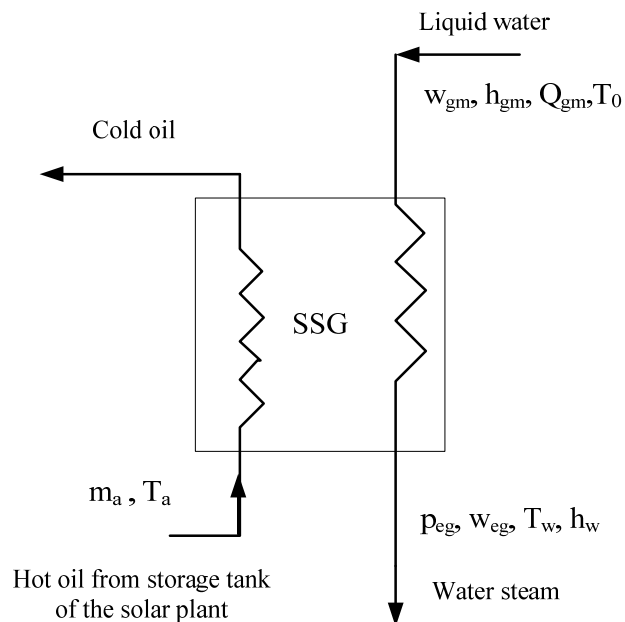
635 **Figures**



636

637

Fig. 1. ISCC diagram.

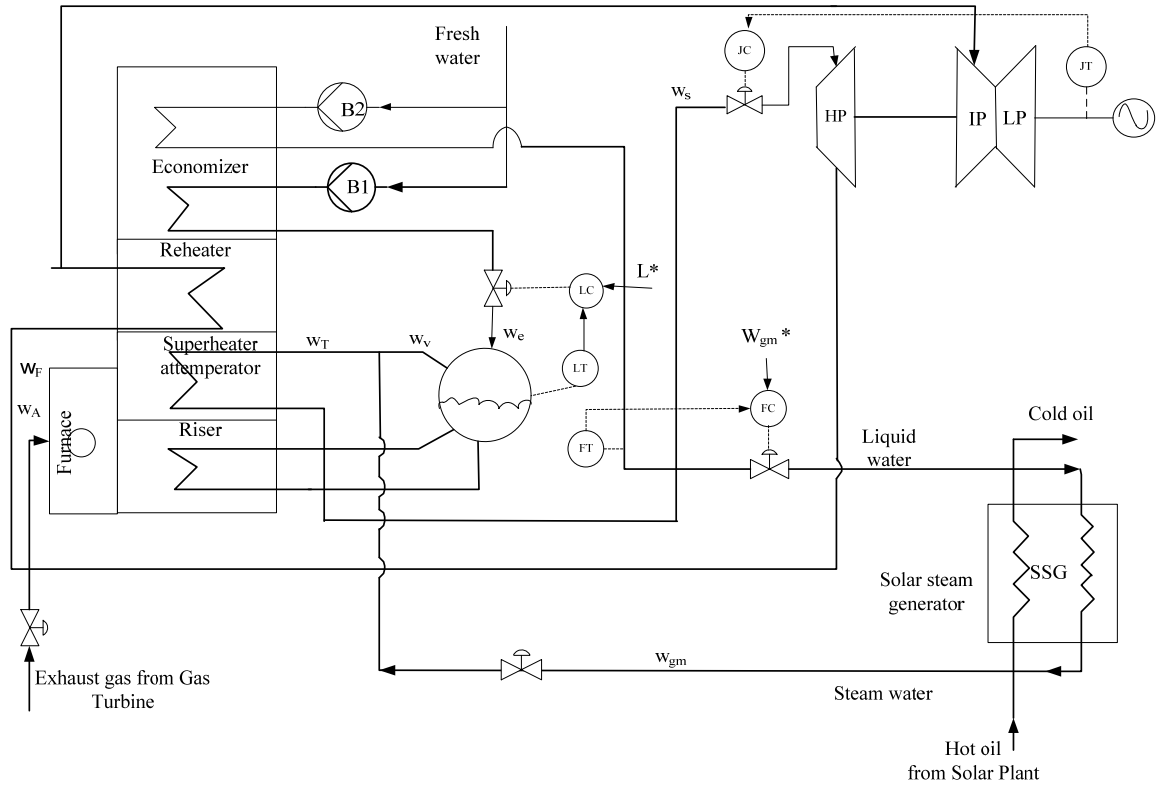


638

639

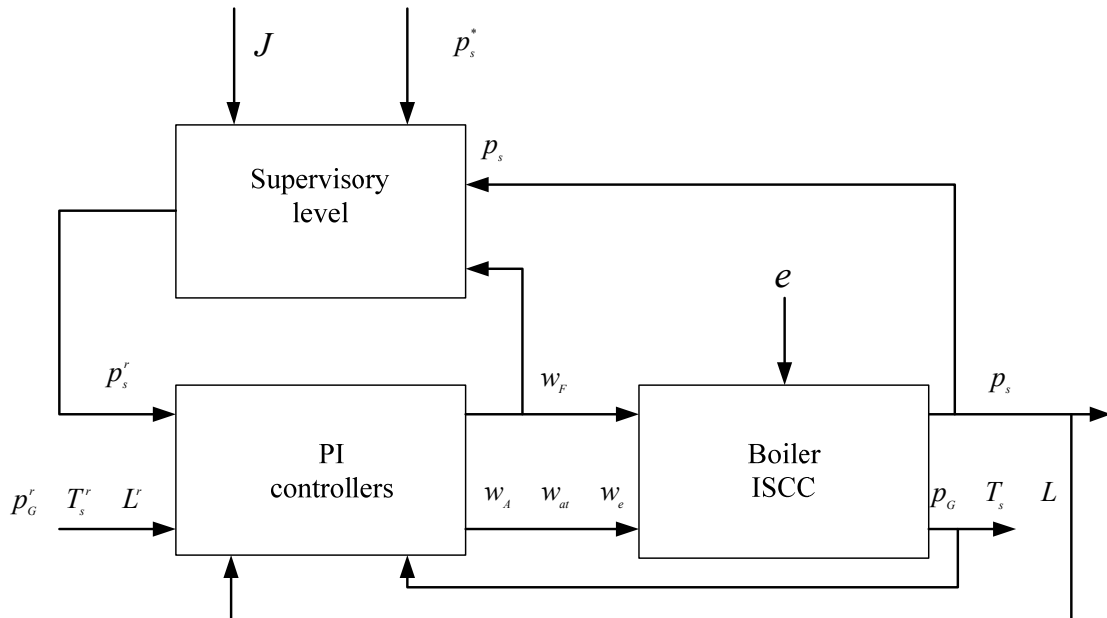
640

Fig. 2. Schematic diagram of the process of heat interchange from the hot oil originating from the solar plant to the steam water injected into the boiler.



641  
642  
643

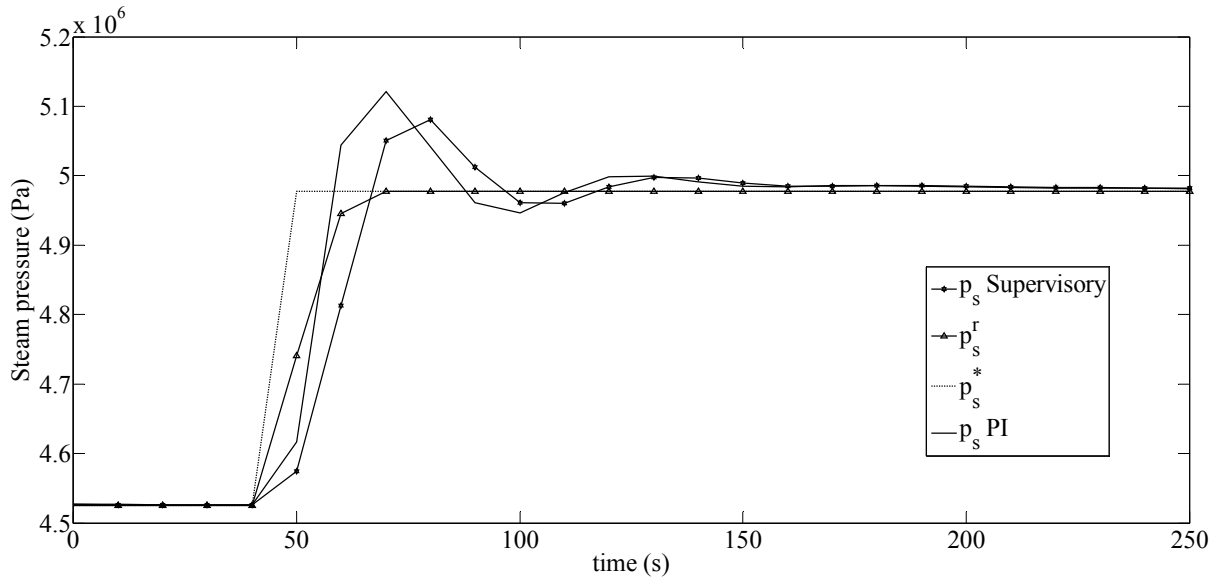
Fig. 3. SSG connected to a CC plant.



644  
645

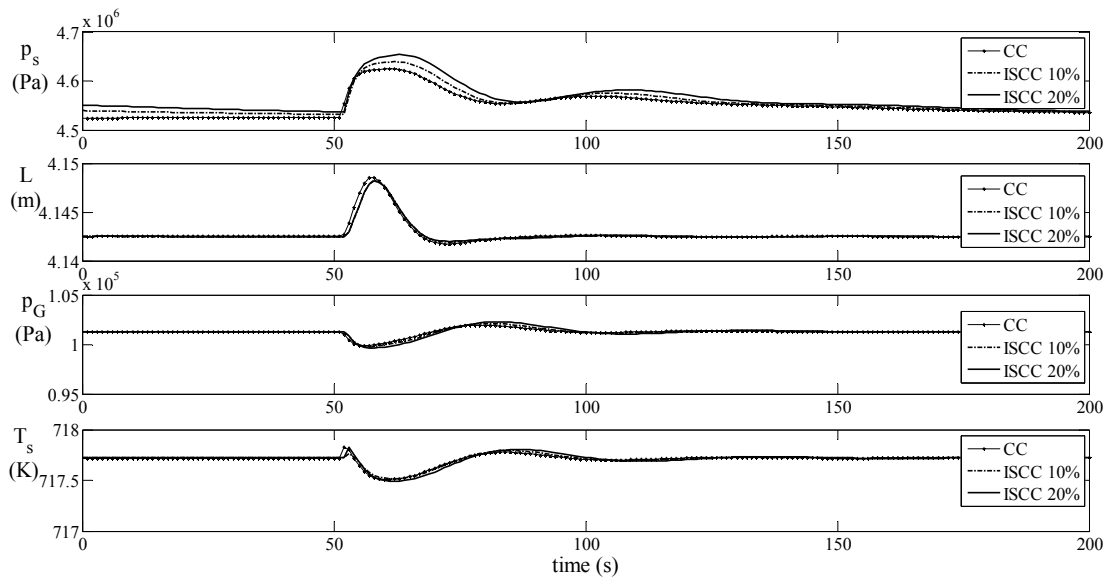
Fig. 4. Control scheme including supervisory level.





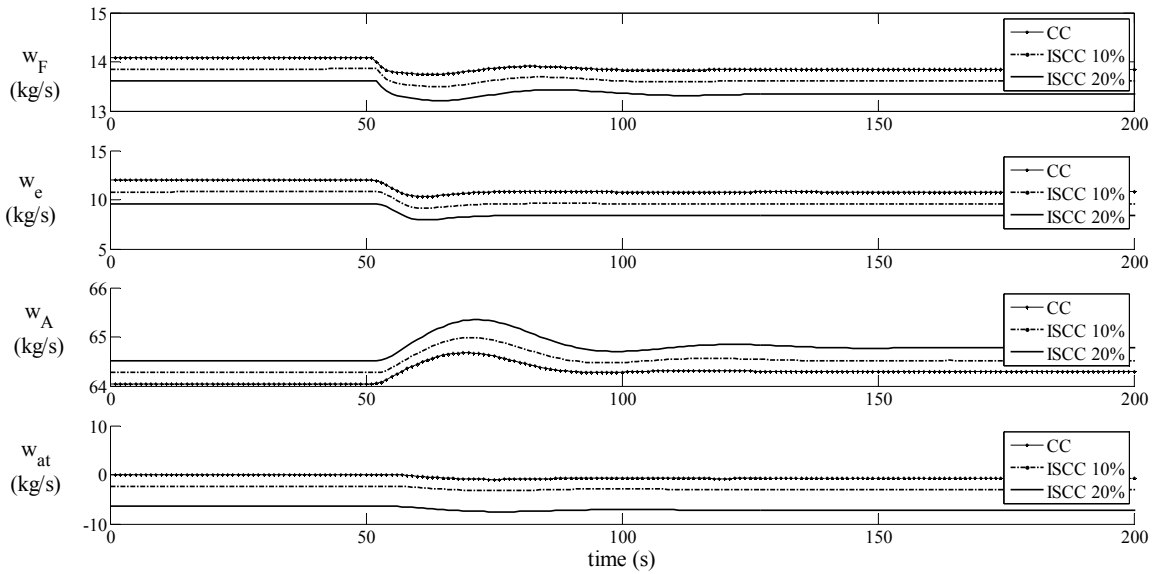
646  
647  
648  
649

Fig. 5. Steam pressure response with a step-function change in the steam pressure set point at 50 s.



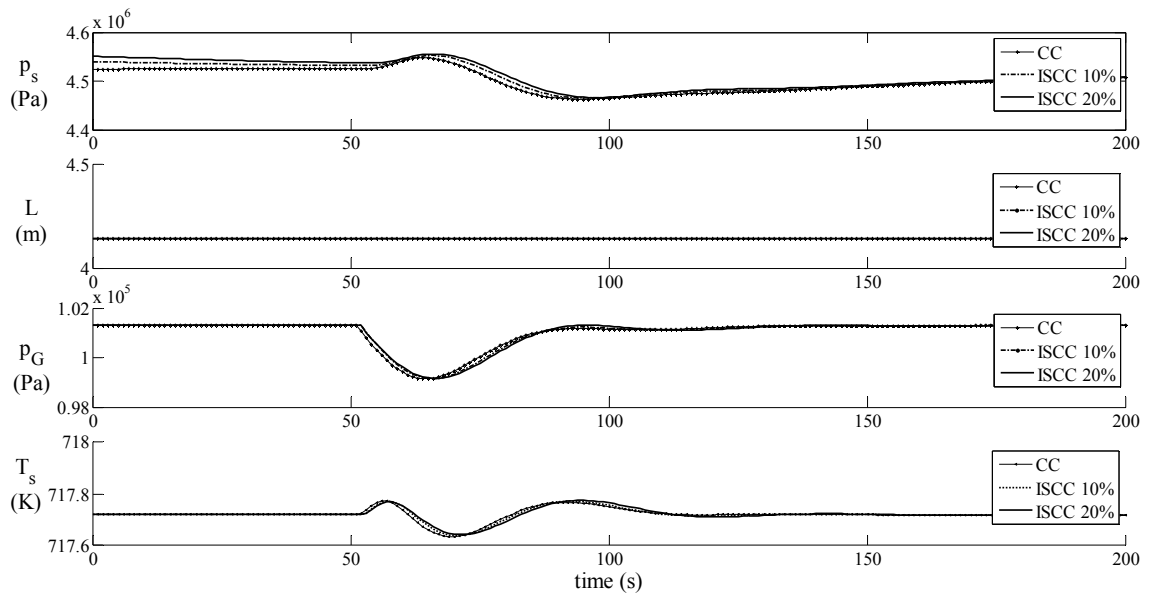
650  
651  
652

Fig. 6. Boiler response to a step-function change in the steam turbine power set point  $P_s^*$  (controlled variables).



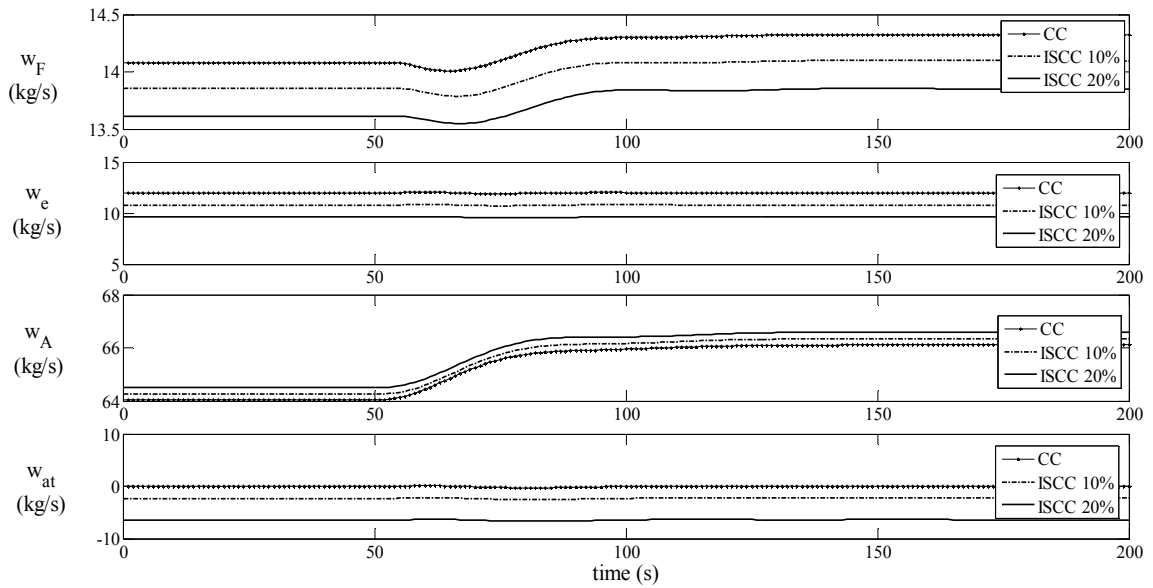
653  
654  
655

Fig. 7. Boiler response to a step-function change in the steam turbine power set point  $P_s^*$  (manipulated variables).



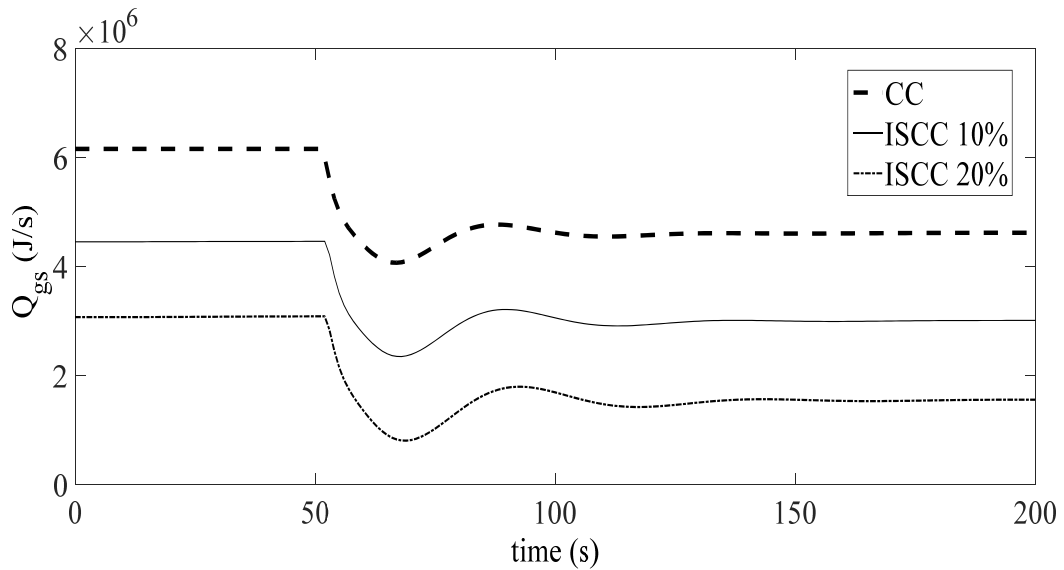
656  
657  
658

Fig. 8. Boiler response to a step-function change in the gas turbine power set point  $P_G^*$  (controlled variables).



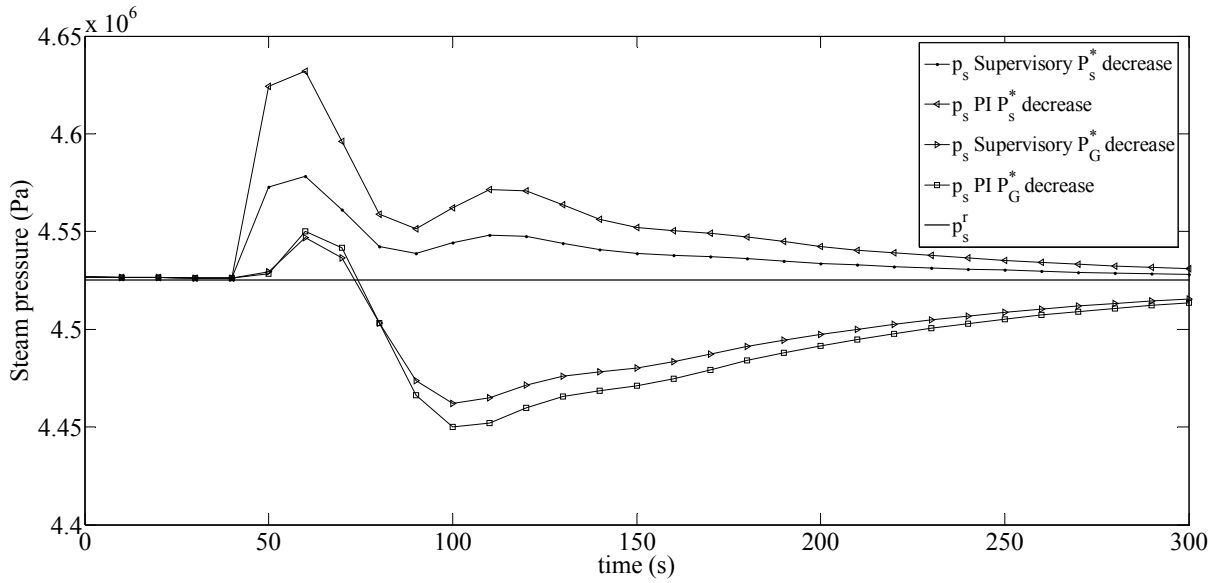
659  
660  
661  
662

Fig. 9. Boiler response to a step-function change in the gas turbine power set point  $P_G^*$  (manipulated variables).



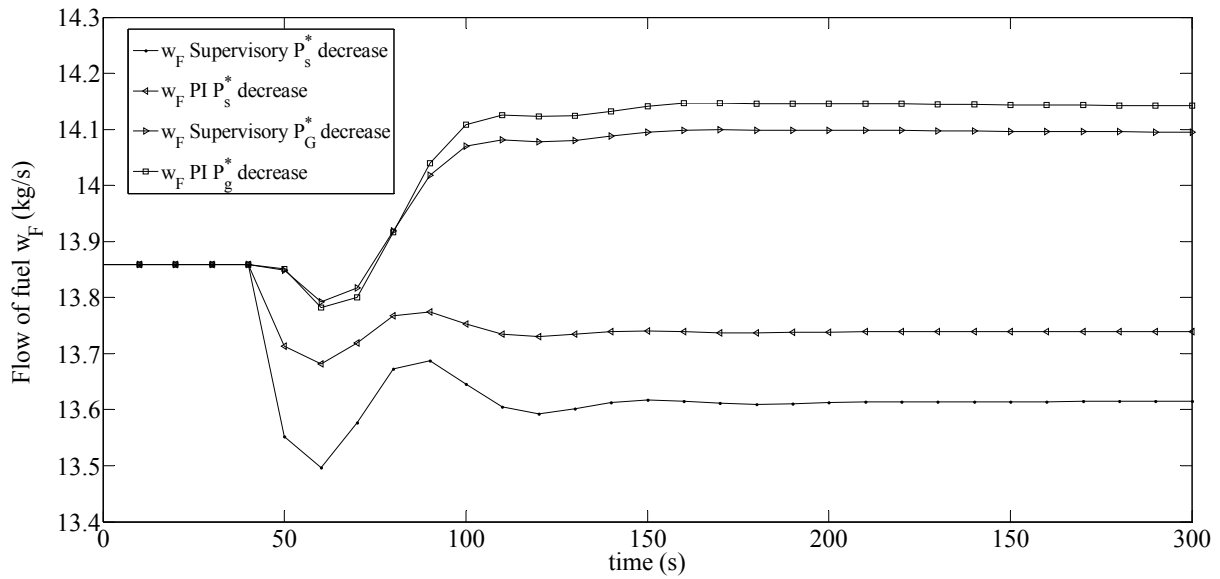
663  
664  
665  
666  
667

Fig. 10. Heat transferred to the superheater when the steam turbine power set point  $P_s^*$  is varied.



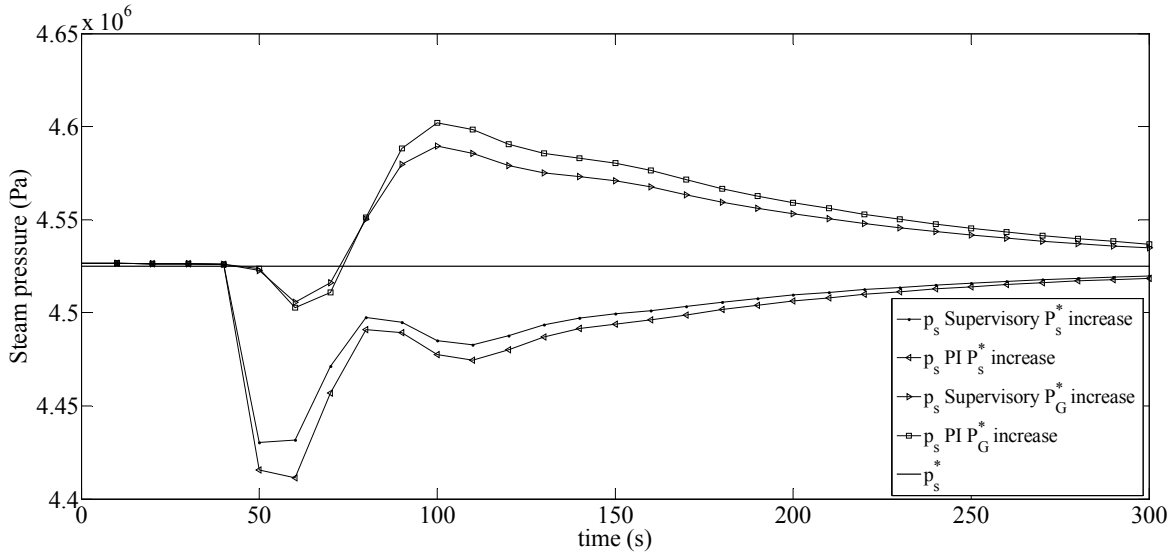
668  
669  
670  
671

Fig. 11. Steam pressure responses to a step-function change (decrease) in the steam turbine power set point ( $P_s^*$ ) and in the gas turbine power set point ( $P_G^*$ ).



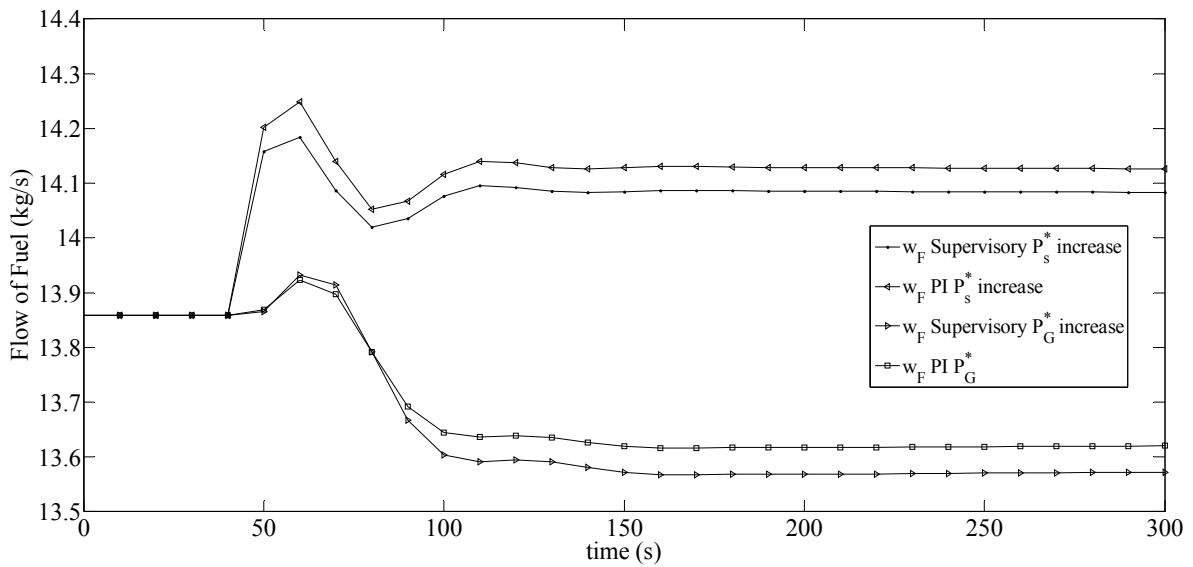
672  
673  
674  
675

Fig. 12. Fuel flow responses, with PI and supervisory controllers, to a step-function change (decrease) in the steam turbine power set point ( $P_s^*$ ) and in the gas turbine power set point ( $P_G^*$ ).



676

677 Fig. 13. Steam pressure responses to a step-function change (increase) in the steam turbine  
678 power set point ( $P_s^*$ ) and in the gas turbine power set point ( $P_G^*$ ).  
679



680

681 Fig. 14. Fuel flow responses to a step-function change (increase) in the steam turbine power set  
682 point ( $P_s^*$ ) and in the gas turbine power set point ( $P_G^*$ ).  
683  
684

685 **Tables**

686 Table 1: Savings achieved using an ISCC plant.

	Fuel savings
10% SSG support	1.7%
20% SSG support	3.7%

687

688

Table 2: Evaluation index  $I_{wF}$

	Supervisory MPC scheme	PI controller	$\Delta I_{wF}$	Savings (%)
$I_{wF}$ kg/s 10%	13.90	13.94	0.04	0.30
$I_{wF}$ kg/s 15%	13.73	13.78	0.05	0.37
$I_{wF}$ kg/s 20%	13.61	13.67	0.06	0.44

689

690

691 Table 3: Savings in fuel consumption between the supervisory MPC and PI control strategies.

	$I_{wF}$ (kg/s), Supervisory MPC strategy	$I_{wF}$ (kg/s), PI controller	$\Delta wF$ (kg)	Savings (%)
$P_s^*$ (-)	13.61	13.74	0.13	0.92
$P_s^*$ (+)	14.09	14.13	0.04	0.30
$P_G^*$ (-)	14.10	14.14	0.05	0.33
$P_G^*$ (+)	13.66	13.76	0.10	0.73

692